Mode locking in periodically forced gradient frequency neural networks

Ji Chul Kim[*] and Edward W. Large

Department of Psychological Sciences and CT Institute for Brain and Cognitive Science, University of Connecticut, Storrs, Connecticut 06269, USA

We study mode locking in a canonical model of gradient frequency neural networks under periodic forcing. The canonical model is a generic mathematical model for a network of nonlinear oscillators tuned to a range of distinct frequencies. It is mathematically more tractable than biological neuron models and allows close analysis of mode-locking behaviors. Here we analyze individual modes of synchronization for a periodically forced canonical model and present a complete set of driven behaviors for all parameter regimes available in the model. Using a closed-form approximation, we show that the Arnold tongue (i.e., locking region) for $k : m$ synchronization gets narrower as k and m increase. We find that numerical simulations of the canonical model closely follow the analysis of individual modes when forcing is weak, but they deviate at high forcing amplitudes for which oscillator dynamics are simultaneously influenced by multiple modes of synchronization.

I. INTRODUCTION

Mode locking is a general phenomenon found in nonlinear physical and biological systems. It refers to the synchronization of oscillations (or modes), with k cycles of one oscillation locked to m cycles of another where k and m are natural numbers [1–3]. Under periodic forcing, nonlinear systems resonate not only at the forcing frequency but also at its harmonics, subharmonics, and integer ratios. In neuroscience, mode locking is observed in periodically stimulated neurons such as squid giant axons [4,5], heart cells [6,7], and pyloric pacemaker neurons [8], which show multiple ratios of locking for varying stimulation frequencies and amplitudes. The dynamics of mode locking has been studied in neuron models of various levels of biophysical detail and abstraction, such as the Hodgkin-Huxley model [9,10], the FitzHugh-Nagumo model [11,12], the Izhikevich model [13], and the integrate-and-fire model [14,15].

Mode locking has been suggested to be an important mechanism for auditory neural processing. Acoustic signals such as speech and music include a wide range of frequencies that carry functionally relevant information. The auditory system transforms them into spatiotemporal patterns of neural activities by processing them through tonotopically organized neural networks [16]. It has been shown that auditory neurons mode lock to acoustic stimulation [17,18], and human auditory brainstem responses include various mode-locking ratios to stimulus frequenices [19]. Mode locking in the auditory system was recently proposed as a basis for the perception of pitch [20], harmony [21,22], tonality [23,24], and rhythm and meter [25–27], which have been traditionally related to frequency ratios (see Sec. IV B for more discussion).

In this paper, we study mode locking in a canonical model of a gradient frequency neural network (GrFNN, pronounced "griffin"), which is a generic mathematical model of tono-topically organized nonlinear neural oscillators [28,29]. It is a canonical model in the sense that a family of biophysically detailed models can be transformed to it via a near-identity change of variables if they satisfy certain assumptions [30]. Thus, the canonical model retains the general properties shared by the detailed models while being mathematically more tractable. The canonical model provides a mathematical framework for building individual realizations with different architectures. Individual GrFNN models can have multiple layers of oscillators that are driven by external signals and connected to other oscillators in the same and/or different layers, and the connections can be either fixed or plastic (e.g., [22,27]). GrFNN models have been used to explain auditory neurophysiological data [31,32] as well as behavioral data on music perception [22,24,27].

Here we perform a dynamical systems analysis of the canonical model under periodic forcing. To analyze driven behaviors closely, we study individual oscillators that are driven by a common signal but are not coupled to each other [33]. Our previous analysis of phase locking (or 1:1 locking) to external forcing showed that the canonical model has multiple parameter regimes that exhibit distinct autonomous and driven behaviors [29]. The goal of the present study is to identify the conditions for stable mode locking for different parameter regimes of the canonical model, and for mode-locking ratios other than 1:1. Unlike biological neuron models, the canonical model allows separate analysis of individual mode-locking ratios because they are represented by different terms in the equation. Below we first describe the canonical model and explain the methods of analysis. Then, we will present the analysis of individual modes and compare it to the numerical simulations of the canonical model.

II. MODEL AND METHODS

A. Canonical model of gradient frequency neural networks

A GrFNN is a network of neural oscillators tuned to a range of distinct frequencies. A canonical model of GrFNNs

─────────
[*]jichulkim21@gmail.com

consisting of oscillators poised near an Andronov-Hopf bifurcation or a Bautin bifurcation [28] is given by

$$\dot{z}_i = z_i\left(a_i + b_i|z_i|^2 + \frac{\epsilon d_i|z_i|^4}{1 - \epsilon|z_i|^2}\right) + \text{RT}_i, \quad (1)$$

where z_i is the complex-valued state of the ith oscillator in the network (subscript $i = 1, \dots, N$), $a_i = \alpha_i + i\omega_i$, $b_i = \beta_{1i} + i\delta_{1i}$, $d_i = \beta_{2i} + i\delta_{2i}$ (α_i, ω_i, β_{1i}, δ_{1i}, β_{2i}, $\delta_{2i} \in \mathbb{R}$; i denotes the imaginary unit), and RT_i is the sum of input terms (see below). The parameters α_i, β_{1i}, and β_{2i} determine the intrinsic amplitude dynamics of the ith oscillator; ω_i is its natural frequency; δ_{1i} and δ_{2i} determine the dependence of intrinsic frequency on amplitude; and $\epsilon > 0$ represents the strength of coupling in the system [34]. As a generic model of neural oscillations, the canonical model represents periodic spikes of neurons as sinusoidal oscillations in the complex plane.

The input to the ith oscillator x_i can include both an external signal $s_i(t)$ and coupling from other oscillators,

$$x_i = s_i(t) + \sum_{j \neq i}^{N} c_{ij} z_j,$$

where c_{ij} is the coupling coefficient [28]. A GrFNN model can include multiple layers of oscillators, and each oscillator can be connected to other oscillators in the same and/or different layers [22,27]. Here we assume $x_i = s_i(t)$ (i.e., no coupling between oscillators) to focus on the dynamics of periodically forced oscillators. We drop the subscript i since we analyze individual oscillators driven by external forcing in isolation. Also, for the simplicity of analysis, we assume that the intrinsic frequency of an oscillator does not depend on its amplitude (i.e., $\delta_{1i} = \delta_{2i} = 0$). Then, Eq. (1) is rewritten as

$$\dot{z} = z\left(\alpha + i\omega + \beta_1|z|^2 + \frac{\epsilon\beta_2|z|^4}{1 - \epsilon|z|^2}\right) + \text{RT}. \quad (2)$$

Since the last intrinsic term (with the coefficient β_2) is a geometric series of high-order terms, the system is bounded only when $\beta_2 < 0$ and $|z| < 1/\sqrt{\epsilon}$.

RT is a sum of resonant terms, which are monomials that capture different modes of synchronization of the oscillator and the input. When input frequency is not known, the canonical model includes all possible resonant monomials. Depending on the actual relationship between the oscillator's natural frequency and the input frequency, only some of the terms in RT become resonant and affect the long-term dynamics of the oscillator while the influence of other terms is averaged out over long timescales (see [28] for more detailed discussions).

A form of RT for an external signal $x(t)$ including a single (but unknown) frequency [28] is given by

$$\begin{aligned}\text{RT} &= x + \sqrt{\epsilon}x\bar{z} + \epsilon x\bar{z}^2 + \epsilon\sqrt{\epsilon}x\bar{z}^3 + \cdots \\ &\quad + \sqrt{\epsilon}x^2 + \epsilon x^2\bar{z} + \epsilon\sqrt{\epsilon}x^2\bar{z}^2 + \epsilon^2 x^2\bar{z}^3 + \cdots \\ &\quad + \epsilon x^3 + \epsilon\sqrt{\epsilon}x^3\bar{z} + \epsilon^2 x^3\bar{z}^2 + \epsilon^2\sqrt{\epsilon}x^3\bar{z}^3 + \cdots \\ &\quad + \epsilon\sqrt{\epsilon}x^4 + \epsilon^2 x^4\bar{z} + \epsilon^2\sqrt{\epsilon}x^4\bar{z}^2 + \epsilon^3 x^4\bar{z}^3 + \cdots \\ &= (x + \sqrt{\epsilon}x^2 + \epsilon x^3 + \epsilon\sqrt{\epsilon}x^4 + \cdots) \\ &\quad \times (1 + \sqrt{\epsilon}\bar{z} + \epsilon\bar{z}^2 + \epsilon\sqrt{\epsilon}\bar{z}^3 + \cdots) \\ &= \frac{x}{1 - \sqrt{\epsilon}x} \cdot \frac{1}{1 - \sqrt{\epsilon}\bar{z}}. \quad (3)\end{aligned}$$

Note that RT is expressed as a product of two geometric series which converge when $|x| < 1/\sqrt{\epsilon}$ and $|z| < 1/\sqrt{\epsilon}$, respectively. Each monomial in RT, which can be expressed as

$$\text{RT}_{k:m} = \epsilon^{(k+m-2)/2} x^k \bar{z}^{m-1},$$

where k and m are natural numbers, represents a different mode of synchronization in the integer ratio of $k : m$. Thus, the resonant monomial for $k = 1$ and $m = 1$ (phase locking) is x, a linear term of the signal only. This term dominates oscillator dynamics when the ratio of the oscillator's natural frequency and the signal frequency is close to 1:1.

In this paper, we first analyze individual modes of synchronization separately by examining a canonical oscillator with a single resonant monomial for $k : m$ locking,

$$\dot{z} = z\left(\alpha + i\omega + \beta_1|z|^2 + \frac{\epsilon\beta_2|z|^4}{1 - \epsilon|z|^2}\right) + \epsilon^{(k+m-2)/2} x^k \bar{z}^{m-1}, \quad (4)$$

where $x(t) = Fe^{i\omega_0 t}$ is an external sinusoidal signal. An analysis of phase locking ($k = 1$, $m = 1$) is given elsewhere [29], and here we focus on harmonic ($k \geqslant 2$, $m = 1$) and subharmonic ($k = 1$, $m \geqslant 2$) locking. Then, we compare the analysis of individual modes with the behavior of canonical oscillators when RT includes the infinite series of resonant monomials in Eq. (3).

B. Analysis of mode-locking behavior

To analyze mode locking of a canonical oscillator, we transform Eq. (4) to the polar coordinates of (r, ψ),

$$\begin{aligned}\dot{r} &= \alpha r + \beta_1 r^3 + \frac{\epsilon\beta_2 r^5}{1 - \epsilon r^2} + \epsilon^{(k+m-2)/2} F^k r^{m-1}\cos\psi, \\ \dot{\psi} &= \Omega - m\epsilon^{(k+m-2)/2} F^k r^{m-2}\sin\psi, \quad (5)\end{aligned}$$

where $z = re^{i\phi}$, $\psi = m\phi - k\omega_0 t$ is the relative phase, and $\Omega = m\omega - k\omega_0$ is the frequency difference. The existence of a stable fixed point in (r, ψ) indicates that the oscillator can mode lock to the input signal in the $k : m$ ratio, with k cycles of the oscillator locked to m cycles of the signal.

The goal of this analysis is to determine the conditions for stable mode locking, which depend on three factors: intrinsic parameters (α, β_1, β_2, and ϵ), input parameters (Ω and F), and the ratio of mode locking (k and m). A previous analysis of the canonical model revealed that the regimes of intrinsic parameters can be categorized into four groups that exhibit qualitatively distinct autonomous and driven behaviors [29]. As shown in Fig. 1 and Table I, each group of parameter regimes has amplitude vector fields of a distinct topology. The first group, represented by the *critical Hopf* regime ($\alpha = 0$, $\beta_1 < 0$), has the spontaneous amplitude of zero (i.e., $r = 0$ is the sole attractor when $F = 0$) due to dr/dt decreasing monotonically as a function of r [Fig. 1(a)]. (As discussed above, $\beta_2 < 0$ for all regimes.) The second group, represented by the *supercritical Hopf* regime ($\alpha > 0$, $\beta_1 < 0$), has a nonzero spontaneous amplitude with dr/dt increasing off the origin and decreasing at higher amplitudes [Fig. 1(b)]. The last two groups include one regime each. The *supercritical double limit cycle* (or DLC) regime ($\alpha < 0$, $\beta_1 > 0$ with a positive
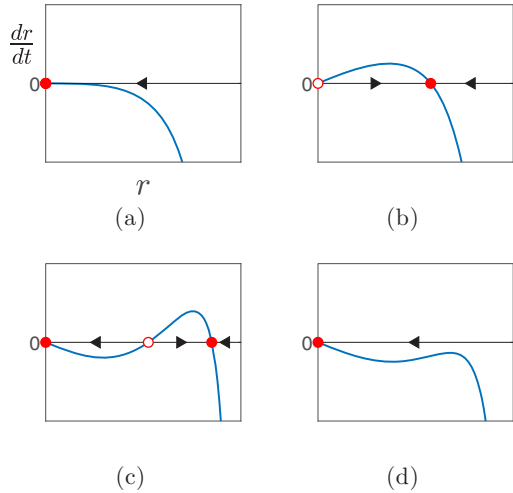
FIG. 1. Autonomous amplitude vector field defined by Eq. (5) when $F = 0$ for (a) the critical Hopf regime, (b) the supercritical Hopf regime, (c) the supercritical DLC regime, and (d) the subcritical DLC regime. Filled and empty circles indicate stable and unstable fixed points, respectively. Arrows indicate the direction of flow.

local maximum in dr/dt) has two spontaneous amplitudes, one zero and one nonzero [Fig. 1(c)]. The *subcritical DLC* regime ($\alpha < 0$, $\beta_1 > 0$ with a negative local maximum in dr/dt) has a sole attractor at zero for autonomous behavior, but unlike the critical Hopf regime, it shows bistable driven behavior because of the "hump" in the vector field [Fig. 1(d)].

Here we examine the mode-locking behavior of canonical oscillators in the four representative parameter regimes, for different ratios of mode locking. As shown below, harmonic locking ($k \geqslant 2$, $m = 1$) does not require a new analysis because it exhibits qualitatively the same dynamics as phase locking ($k = 1$, $m = 1$). Thus, the present analysis focuses on subharmonic locking ($k = 1$, $m \geqslant 2$).

The analysis of individual modes is organized as follows. For each subharmonic ratio of interest, we examine the four regimes of intrinsic parameters listed above as to whether a canonical oscillator mode locks to a given sinusoidal signal of

TABLE I. Groups of intrinsic parameter regimes with distinct autonomous and driven behaviors. $\beta_2 < 0$ for all regimes.

Group	α	β_1	Local extrema[a]	Regime
1	0	0	None	
	0	−	"	Critical Hopf
	−	0	"	
	−	−	"	
	−	+	"	
2	0	+	Positive max	
	+	0	"	
	+	−	"	Supercritical Hopf
	+	+	"	
3	−	+	Negative min, positive max	Supercritical DLC
4	−	+	Negative min, negative max	Subcritical DLC

[a]Local extrema of dr/dt in the autonomous amplitude vector field defined by Eq. (5) when $F = 0$ (see Fig. 1).

frequency ω_0 and amplitude F. This is done by identifying the regions of the (Ω, F) space where stable nonzero fixed points (r^*, ψ^*) exist (the stability regions are called *Arnold tongues*). The methods for analysis and numerical simulation are given below.

1. Stability analysis of fixed points

For a given frequency difference Ω and input amplitude F, we examine whether a canonical oscillator mode locks to the external input or not by performing a stability analysis of fixed points. First, we get fixed points (r^*, ψ^*) by solving the steady-state equations $\dot{r} = 0$ and $\dot{\psi} = 0$ for Eq. (5). By eliminating ψ^*, we get

$$\left(\alpha + \beta_1 r^{*2} + \frac{\epsilon \beta_2 r^{*4}}{1 - \epsilon r^{*2}} \right)^2 + \left(\frac{\Omega}{m} \right)^2 = \epsilon^{k+m-2} F^{2k} r^{*2m-4},$$

(6)

which is expanded into a polynomial equation of r^* of the order eight if $m \leqslant 4$ or $2m$ if $m \geqslant 5$. We solve this equation by numerical root finding. Then, we determine the linear stability of each fixed point (i.e., if it is a stable or unstable node, a stable or unstable spiral, or a saddle point) by evaluating the Jacobian matrix of Eq. (5) [29,35].

2. Stability of zero

It is obvious from Eq. (4) that $z = 0$ is always a fixed point for $m \geqslant 2$ regardless of the external input x. This is an important difference from $m = 1$ for which zero is not a fixed point unless $F = 0$. Since phase is indeterminate at zero, the stability of the zero solution only requires $r^* = 0$ to be attracting. Also, the linear stability analysis at zero may be indecisive when the linear coefficient α is zero. Thus, the linear stability analysis described above is not always adequate for determining the stability of the zero solution. We examine each case closely and choose appropriate methods of analysis as described in Sec. III B.

3. Calculation of Arnold tongue boundary

An Arnold tongue is the region of a parameter space in which a forced system mode locks to the input at a certain integer ratio [36,37]. In this paper, we identify Arnold tongues for canonical oscillators in the input parameter space (Ω, F). The stability analysis described above finds Arnold tongues by examining a dense array of points in (Ω, F) for the existence of stable nonzero fixed points. Additionally, we corroborate this analysis by identifying the border of Arnold tongues with an alternative method.

We cannot solve Eq. (6) analytically, but we can show how many real roots it has by treating them as intersections of the following two functions:

$$y_1 = \left(\alpha + \beta_1 X + \frac{\epsilon \beta_2 X^2}{1 - \epsilon X} \right)^2,$$

$$y_2 = \epsilon^{k+m-2} F^{2k} X^{m-2} - \left(\frac{\Omega}{m} \right)^2,$$

(7)

where $X \equiv r^{*2}$. Note that y_1 depends on the intrinsic parameters only, whereas y_2 depends on the input parameters. We

identify the border of Arnold tongues for subharmonic locking by numerically calculating the frequency difference Ω for which y_1 and y_2 are tangent to each other. This is the border for the existence of fixed point(s), but it is also the border for stable mode locking because, as shown in Sec. III B, there is always one stable fixed point if one or more fixed points exist. The Arnold tongues for harmonic locking have the same properties as those for phase locking, a detailed analysis of which is given elsewhere [29].

4. Numerical integration

In addition to the steady-state analyses described above, we used numerical integration to examine non-steady-state trajectories and to confirm analytic results. We used the GrFNN Toolbox [38] to solve the canonical model by the Runge-Kutta fourth-order method with a fixed time step. The time step for each simulation was chosen so that the sampling rate is 20 times the highest frequency in the model (either the input frequency or the highest natural frequency).

To identify the Arnold tongues for the canonical model with the infinite-series RT, we ran a one-layer GrFNN model multiple times for different forcing amplitudes and computed the average instantaneous frequencies of the oscillators after initial transients. This gave us a two-dimensional matrix of average instantaneous frequencies, with the dimensions of natural frequency ω and forcing amplitude F. A point in the (ω, F) space was deemed part of an Arnold tongue (1) if the average instantaneous frequency was close to an integer ratio of the input frequency, and (2) if it was close to the instantaneous frequencies of its neighbors in the parameter space (see Sec. IV C). An instantaneous frequency was judged to be "close" to a target frequency if their distance was smaller than a half of the distance between adjacent natural frequencies. Distances between frequencies were measured in log difference because the natural frequencies were equally spaced on a logarithmic scale.

III. ANALYSIS OF INDIVIDUAL MODES

A. Harmonic locking ($k > 1, m = 1$)

When $m = 1$, a canonical oscillator with a single-monomial input is governed by

$$\dot{z} = z\left(\alpha + i\omega + \beta_1|z|^2 + \frac{\epsilon\beta_2|z|^4}{1 - \epsilon|z|^2}\right) + \epsilon^{(k-1)/2}x^k.$$

When $x = Fe^{i\omega_0 t}$, the monomial is written as

$$x'(t) = \epsilon^{(k-1)/2}x^k = \epsilon^{(k-1)/2}F^k e^{ik\omega_0 t},$$

which can be considered an external signal of amplitude $\epsilon^{(k-1)/2}F^k$ and frequency $k\omega_0$. Since the monomial is a linear term of an external signal only, the model is equivalent to a canonical oscillator with a monomial for $k = 1$ and $m = 1$ (phase locking), but for the new input $x'(t)$. A detailed analysis is given elsewhere for canonical oscillators phase locking to external forcing [29], and hence harmonic locking does not require a new analysis. By the same token, mode locking at the integer ratio of $k : m$ ($k \geqslant 2, m \geqslant 2$) exhibits the same dynamical properties as subharmonic locking at $1 : m$, which we discuss below.

B. Subharmonic locking ($k = 1, m > 1$)

1. Second subharmonic ($m = 2$)

Subharmonic locking in canonical oscillators is different in important ways for $m = 2$ from other subharmonic numbers. Also, the equations for $m = 2$ are more tractable and allow closer analysis. Let us first examine the properties of mode locking that are common to all parameter regimes and then discuss each regime for its distinct properties.

When $m = 2$, Eq. (5) is rewritten as

$$\dot{r} = \alpha r + \beta_1 r^3 + \frac{\epsilon\beta_2 r^5}{1 - \epsilon r^2} + (\sqrt{\epsilon}F)^k r \cos\psi, \quad (8)$$

$$\dot{\psi} = \Omega - 2(\sqrt{\epsilon}F)^k \sin\psi. \quad (9)$$

Note that Eq. (9) does not include oscillator amplitude r or intrinsic parameters α, β_1, and β_2. Thus, the dynamics of relative phase ψ is independent of amplitude dynamics and is identical across different regimes of intrinsic parameters.

Equation (9) is a well-known equation for a nonuniform oscillator known as the Adler equation [35,39], and its simple form allows a close analysis of phase dynamics. First, the steady-state equation $\dot{\psi} = 0$ indicates that the steady-state solution

$$\sin\psi^* = \frac{\Omega}{2(\sqrt{\epsilon}F)^k}$$

exists if

$$|\Omega| \leqslant 2(\sqrt{\epsilon}F)^k, \quad (10)$$

which defines the locking region for ψ in the (Ω, F) plane [see the red dashed lines in panel (a) of Figs. 2–5]. Second, we can solve Eq. (9) analytically and express ψ as an explicit function of time [39] (see also [40]). Inside the locking region, relative phase approaches a steady-state value monotonically, indicating stable mode locking. Outside the locking region, relative phase does not converge but makes full rotations with a bottleneck near $\frac{\pi}{2}$ if $\Omega > 0$ or near $-\frac{\pi}{2}$ if $\Omega < 0$. As shown below, however, the locking region for ψ can be different from the Arnold tongue, defined here as the region with stable nonzero fixed points, because $r^* = 0$ can be the only stable fixed point in some part of the region with stable ψ^*.

The stability of the zero solution for $m = 2$ also allows a close analysis. Equation (8) defines a vector field and determines whether r increases or decreases at a given value of r. Inside the locking region where stable ψ^* exists, the linear coefficient of r in the right-hand side of Eq. (8), $\alpha + (\sqrt{\epsilon}F)^k \cos\psi$, approaches a steady-state value, and its sign determines the stability of the zero solution (stable if negative and unstable if positive) because the linear term dominates the equation when $r \approx 0$. Since $\cos\psi^* > 0$ for stable ψ^*, zero is unstable if $\alpha \geqslant 0$ regardless of ψ^*. For $\alpha < 0$, zero is stable if $|\alpha| > (\sqrt{\epsilon}F)^k$ (weak forcing) regardless of ψ^*. If $|\alpha| \leqslant (\sqrt{\epsilon}F)^k$ (strong forcing), zero is stable when

$$|\Omega| > 2\sqrt{(\sqrt{\epsilon}F)^{2k} - \alpha^2}, \quad (11)$$

because $\cos\psi^* = \sqrt{1 - \sin^2\psi^*}$ for stable ψ^*. Equation (11) defines the boundary between the "NZ/Z" region (where nonzero and zero attractors coexist) and the "NZ" region
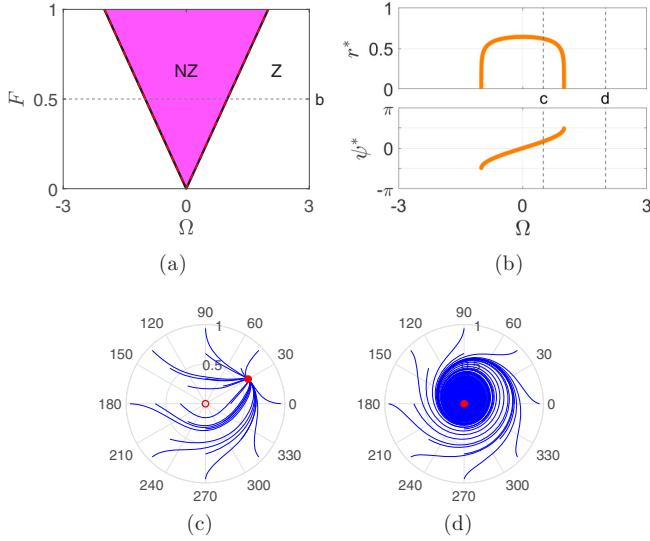
(a)

(b)

(c)

(d)

FIG. 2. 1:2 mode locking of a critical Hopf oscillator ($\alpha = 0$, $\beta_1 = -0.5$, $\beta_2 = -1$, $\epsilon = 1$). (a) The Arnold tongue bounded by black solid lines obtained with Eq. (7) and the locking region for ψ bounded by red dashed lines given by Eq. (10) shown with regions of the (Ω, F) space labeled by attractor set (NZ: stable nonzero fixed point; Z: stable zero). See Fig. 10 for the color scheme for all attractor sets. (b) The stability of nonzero fixed points (r^*, ψ^*) for $F = 0.5$. Orange color indicates stable nodes. (c) Trajectories in (r, ψ) starting from different initial conditions when the driven oscillator is inside the locking region ($\Omega = 0.5$, $F = 0.5$). Filled and empty red circles show stable and unstable fixed points, respectively. (d) Trajectories outside the locking region ($\Omega = 2$, $F = 0.5$). Horizontal and vertical dashed lines indicate the parameter values used in other panels identified with letter labels.

(where only a nonzero attractor exists) in Figs. 4(a) and 5(a). The linear stability analysis of the zero solution is consistent with this analysis and shows that zero is a node when it is stable and a saddle point when unstable. This is expected given that ψ approaches ψ^* monotonically.

Outside the locking region where ψ rotates, the stability of the zero solution can be determined by integrating Eq. (8) while ψ makes one 2π rotation after a small perturbation from zero. Since the trajectory of ψ for the solution of Eq. (9) is symmetrical about $\pm\frac{\pi}{2}$ [39], the integral of $\cos\psi$ evaluated over one period is zero. Thus, we find that for small enough perturbations, oscillator amplitude is attracted back to zero if the lowest-order intrinsic term has a negative coefficient. This is when a spontaneous amplitude of the oscillator is zero (see Fig. 1). Thus, zero is stable outside the locking region for the critical ($\alpha = 0$, $\beta_1 < 0$) and both DLC ($\alpha < 0$, $\beta_1 > 0$) regimes and unstable for the supercritical Hopf regime ($\alpha > 0$, $\beta_1 < 0$) [see panel (a) of Figs. 2–5].

a. Critical Hopf regime. A stability analysis of fixed points shows that a critical Hopf oscillator always has one nonzero fixed point inside the locking region for ψ given by Eq. (10) [see Fig. 2(a)], and the fixed point is always a stable node [Figs. 2(b) and 2(c)]. Thus, the Arnold tongue (bounded by black solid lines) coincides with the region with stable ψ^* (bounded by red dashed lines). As discussed above, the zero solution is unstable inside the locking region because
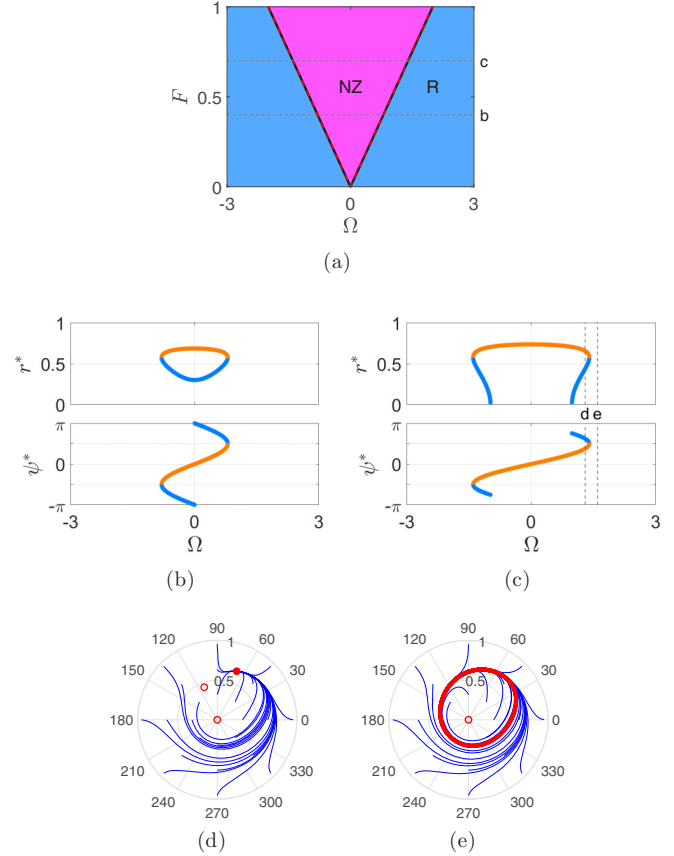

(a)

(b)

(c)

(d)

(e)

FIG. 3. 1:2 mode locking of a supercritical Hopf oscillator ($\alpha = 0.5$, $\beta_1 = -1$, $\beta_2 = -1$, $\epsilon = 1$). See Fig. 2 for a detailed caption. (a) The Arnold tongue and the locking region for ψ shown with regions of (Ω, F) labeled by attractor set (NZ: stable nonzero fixed point; R: stable limit cycle or rotation). (b) The stability of nonzero fixed points for $F = 0.4$ (orange: stable node, blue: saddle point; a hint for the grayscale version: the node has a higher amplitude than the saddle when both exist for given Ω) and (c) for $F = 0.7$. (d) Trajectories in (r, ψ) inside the locking region ($\Omega = 1.3$, $F = 0.7$) and (e) outside the locking region ($\Omega = 1.6$, $F = 0.7$). The red closed orbit indicates a limit-cycle attractor.

$\alpha = 0$, and it is stable outside the locking region because spontaneous amplitude is zero [see Figs. 2(a), 2(c), and 2(d)].

b. Supercritical Hopf regime. Inside the Arnold tongue, which coincides with the region with stable ψ^*, a supercritical Hopf oscillator can have up to two nonzero fixed points, and one of them is always a stable node [Figs. 3(b) and 3(c)]. A saddle-node bifurcation on invariant circle (or SNIC bifurcation) occurs at the mode-locking boundary where a stable node and a saddle point collide and disappear leaving a stable limit cycle that encompasses the origin [Figs. 3(d) and 3(e)]. Thus, outside the locking region, relative phase makes 2π rotations while amplitude fluctuates around the spontaneous amplitude. Zero is an unstable fixed point both in and out of the locking region due to positive α as discussed above.

c. Supercritical DLC regime. Inside the Arnold tongue, a supercritical DLC oscillator can have up to four fixed points, but only one is stable which is always a node [Figs. 4(b)–4(d)].
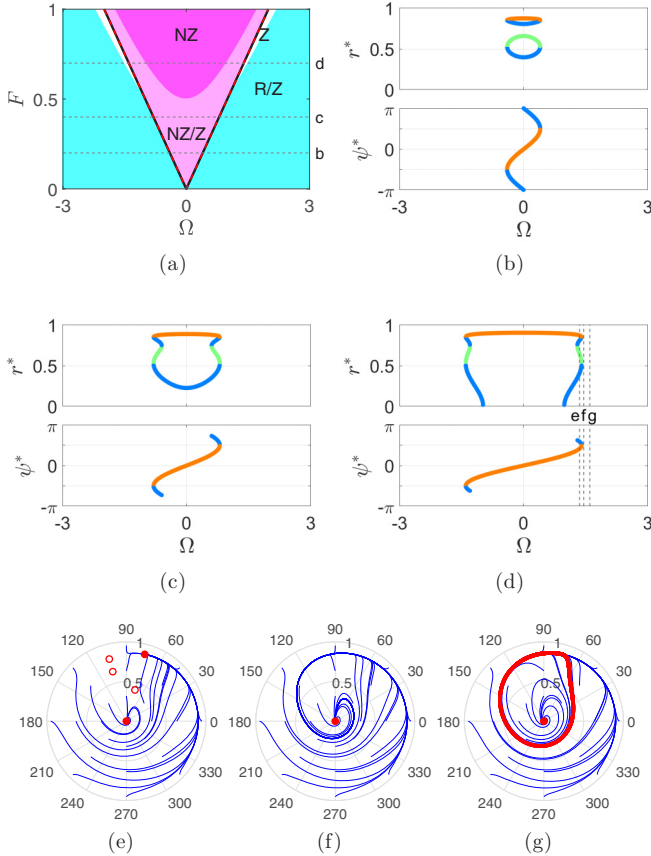
FIG. 4. 1:2 mode locking of a supercritical DLC oscillator ($\alpha = -0.5$, $\beta_1 = 2$, $\beta_2 = -0.5$, $\epsilon = 1$). See Fig. 2 for a detailed caption. (a) The Arnold tongue and the locking region for ψ shown with regions of (Ω, F) labeled by attractor set (NZ: stable nonzero fixed point; Z: stable zero; R: stable limit cycle or rotation). (b) The stability of nonzero fixed points for $F = 0.2$ (orange: stable node; green: unstable node; blue: saddle point; for the grayscale version: when there are four fixed points for given Ω, the one with the highest amplitude is a stable node, followed by a saddle, an unstable node, and another saddle), (c) for $F = 0.4$, and (d) for $F = 0.7$. (e) Trajectories in (r, ψ) inside the locking region ($\Omega = 1.35$, $F = 0.7$), (f) just outside the locking region ($\Omega = 1.45$, $F = 0.7$), and (g) further outside ($\Omega = 1.6$, $F = 0.7$). The red closed orbit indicates a stable limit cycle.

A saddle-node bifurcation occurs at the locking boundary, but for strong forcing it does not leave a stable limit cycle (i.e., not a SNIC bifurcation), making zero a global attractor [see Figs. 4(e) and 4(f), and the narrow region labeled Z in Fig. 4(a)]. Further away from the locking boundary, a stable limit cycle appears around stable zero indicating a double limit cycle bifurcation in (r, ψ) [Figs. 4(f) and 4(g)]. For weaker forcing, a stable limit cycle appears right outside the locking boundary, indicating a SNIC bifurcation. Zero is always stable outside the locking region because $\alpha < 0$. Inside, it is a local attractor in the region of weak forcing or large frequency difference [labeled NZ/Z in Fig. 4(a)], which is given by Eq. (11).

d. Subcritical DLC regime. Figure 5(a) shows that the Arnold tongue (bounded by the black solid lines) for a subcritical DLC oscillator is lifted off $F = 0$ and does not
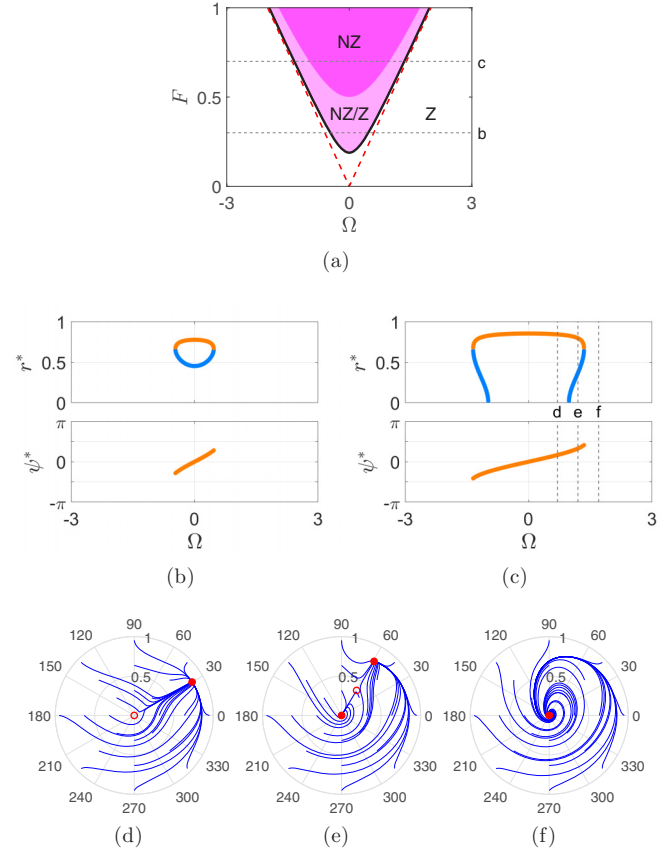

FIG. 5. 1:2 mode locking of a subcritical DLC oscillator ($\alpha = -0.5$, $\beta_1 = 1.1$, $\beta_2 = -0.5$, $\epsilon = 1$). See Fig. 2 for a detailed caption. (a) The Arnold tongue and the locking region for ψ shown with regions of (Ω, F) labeled by attractor set (NZ: stable nonzero fixed point; Z: stable zero). (b) The stability of nonzero fixed points for $F = 0.3$ (orange, higher amplitude: stable node; blue, lower amplitude: saddle point) and (c) for $F = 0.7$. (d) Trajectories in (r, ψ) well inside the locking region ($\Omega = 0.7$, $F = 0.7$), (e) just inside the locking region ($\Omega = 1.2$, $F = 0.7$), and (f) outside the locking region ($\Omega = 1.7$, $F = 0.7$).

coincide with the locking region for ψ (the red dashed lines) because zero is a global attractor for weak forcing. Inside the Arnold tongue, a subcritical DLC oscillator can have up to two nonzero fixed points, one of which is always a stable node [Figs. 5(b) and 5(c)]. Zero is stable in the region given by Eq. (11). A saddle-node bifurcation occurs at the locking boundary, outside which zero is the only attractor.

Figure 5 suggests that zero is stable inside the Arnold tongue when a nonzero saddle point exists. Moving from the NZ region to the NZ/Z region in Fig. 5(a), zero gains stability as a saddle point separates from it [Figs. 5(c)–5(e)]. Note that the stable manifold of the saddle serves as the basin boundary for the zero and nonzero attractors [Fig. 5(e)]. The same relationship is observed for the supercritical DLC regime: Zero is stable inside the locking region when a nonzero saddle point exists (Fig. 4). However, this does not apply to the supercritical Hopf regime for which zero is unstable with or without a nonzero saddle (Fig. 3). It appears that this rule holds for the regimes where a spontaneous amplitude is zero
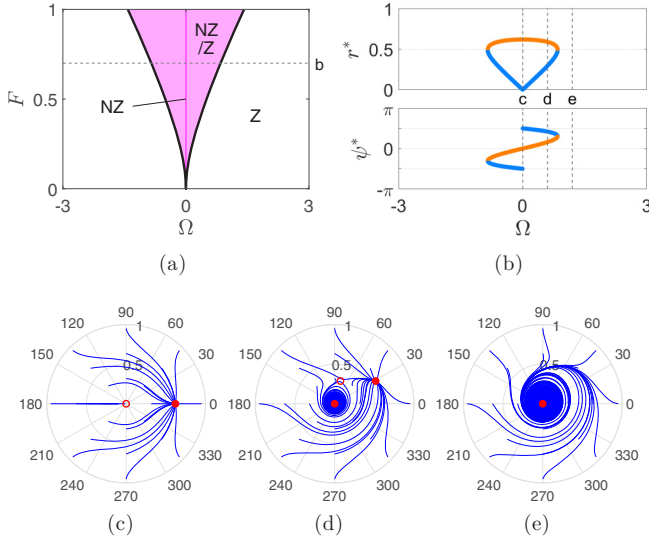
(a)

(b)

(c)

(d)

(e)

FIG. 6. 1:3 mode locking of a critical Hopf oscillator ($\alpha = 0$, $\beta_1 = -0.5$, $\beta_2 = -1$, $\epsilon = 1$). See Fig. 2 for a detailed caption. (a) The Arnold tongue shown with regions of (Ω, F) labeled by attractor set (NZ: stable nonzero fixed point; Z: stable zero). (b) The stability of nonzero fixed points (r^*, ψ^*) for $F = 0.7$ (orange, higher amplitude: stable node; blue, lower amplitude: saddle point). (c) Trajectories in (r, ψ) when $\Omega = 0$ ($F = 0.7$), (d) inside the locking region with $\Omega \neq 0$ ($\Omega = 0.6$, $F = 0.7$), and (e) outside the locking region ($\Omega = 1.2$, $F = 0.7$).

(i.e., zero is an attractor when $F = 0$). The critical Hopf regime satisfies this rule because zero is unstable inside the Arnold tongue where no nonzero saddle exists (Fig. 2). We show below that the same rule holds for $m \geqslant 3$.

2. Third subharmonic ($m = 3$)

Unlike $m = 2$, the phase dynamics for $m = 3$ is not independent of amplitude dynamics because the differential equation for ψ includes r [see Eq. (5)]. Hence, the closed-form analysis done for $m = 2$ is unavailable for $m = 3$, and here we determine the mode-locking behavior of canonical oscillators by analyzing the stability of fixed points and examining trajectories in the phase space.

a. Critical Hopf regime. Inside the Arnold tongue, a critical Hopf oscillator shows bistability with zero and nonzero attractors except when $\Omega = 0$ for which zero is unstable (Fig. 6). Note that zero is stable inside the locking region when a nonzero saddle point exists, satisfying the rule found for $m = 2$ (see Sec. III B 1 d). A saddle-node bifurcation occurs at the locking boundary, outside which zero is the only attractor [Figs. 6(b), 6(d), and 6(e)].

b. Supercritical Hopf regime. The mode-locking behavior of a supercritical Hopf oscillator for $m = 3$ is basically identical to the behavior for $m = 2$. It has a nonzero attractor (a stable node) inside the locking region, and a stable limit cycle emerging via a SNIC bifurcation is the only attractor outside the locking boundary (Fig. 7). Zero is an unstable fixed point in the entire (Ω, F) space. The only difference from $m = 2$ is that a nonzero saddle always exists inside the locking region
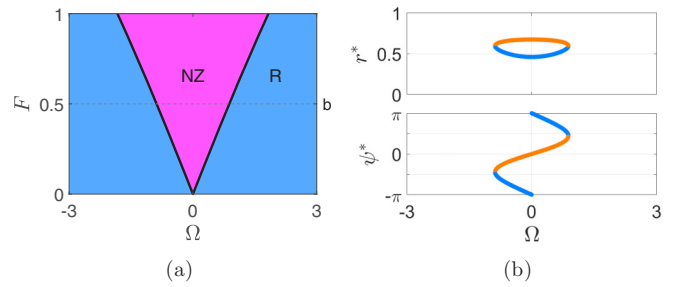

(a)

(b)

FIG. 7. 1:3 mode locking of a supercritical Hopf oscillator ($\alpha = 0.5$, $\beta_1 = -1$, $\beta_2 = -1$, $\epsilon = 1$). See Fig. 2 for a detailed caption. (a) The Arnold tongue shown with regions of (Ω, F) labeled by attractor set (NZ: stable nonzero fixed point; R: stable limit cycle or rotation). (b) The stability of nonzero fixed points for $F = 0.5$ (orange, higher amplitude: stable node; blue, lower amplitude: saddle point).

[Fig. 7(b); cf. Figs. 3(b) and 3(c)], but this does not cause any qualitative difference in mode-locking behavior.

c. Supercritical DLC regime. There are two main differences for a supercritical DLC oscillator with $m = 3$ compared to $m = 2$. First, zero is always stable in and out of the Arnold tongue [Fig. 8(a); cf. Fig. 4(a)]. Along with the attractor at zero, a stable node exists inside the locking region, whereas a limit-cycle attractor (rotation) exists outside the locking region. The stability of zero in the entire Arnold tongue can be related to the observation that a nonzero saddle does not disappear for strong forcing when $m = 3$ [Fig. 8(b); cf. Fig. 4(d)]. A second difference from $m = 2$ is that a SNIC bifurcation occurs at the locking boundary regardless of forcing amplitude. Thus, rotation is always an attractor along with stable zero outside the locking boundary [i.e., no Z region in Fig. 8(a); cf. Fig. 4(a)].

d. Subcritical DLC regime. Zero is a local attractor in the entire Arnold tongue for a subcritical DLC oscillator when $m = 3$ [Fig. 9(a); cf. Fig. 5(a)], which can be explained by the presence of a nonzero saddle point [Fig. 9(b); cf. Fig. 5(c)]. Like $m = 2$, zero is a global attractor outside the tongue.
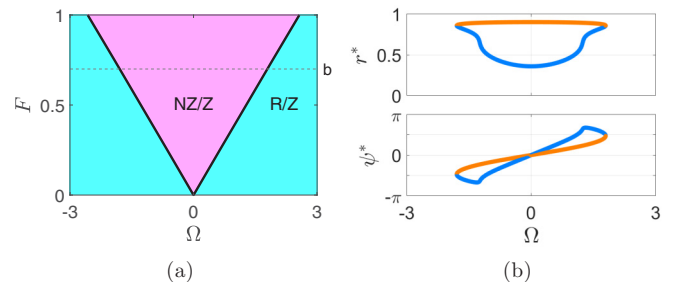

(a)

(b)

FIG. 8. 1:3 mode locking of a supercritical DLC oscillator ($\alpha = -0.5$, $\beta_1 = 2$, $\beta_2 = -0.5$, $\epsilon = 1$). See Fig. 2 for a detailed caption. (a) The Arnold tongue shown with regions of (Ω, F) labeled by attractor set (NZ: stable nonzero fixed point; Z: stable zero; R: stable limit cycle or rotation). (b) The stability of nonzero fixed points for $F = 0.7$ (orange, higher amplitude: stable node; blue, lower amplitude: saddle point). Similar to $m = 2$, there can be up to four nonzero fixed points for weaker forcing [see Figs. 4(b) and 4(c)].
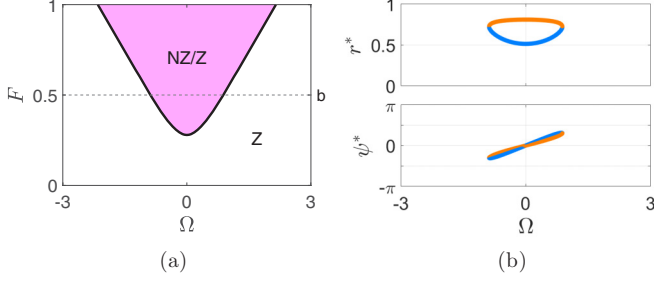
FIG. 9. 1:3 mode locking of a subcritical DLC oscillator ($\alpha = -0.5$, $\beta_1 = 1.1$, $\beta_2 = -0.5$, $\epsilon = 1$). See Fig. 2 for a detailed caption. (a) The Arnold tongue shown with regions of (Ω, F) labeled by attractor set (NZ: stable nonzero fixed point; Z: stable zero). (b) The stability of nonzero fixed points (r^*, ψ^*) for $F = 0.5$ (orange, higher amplitude: stable node; blue, lower amplitude: saddle point).

3. Summary: Subharmonic locking

Figure 10 compares the Arnold tongues for all four representative regimes of intrinsic parameters for $m = 2$, 3, and 4. The figure shows that the set of attractors available in the regions of (Ω, F) is identical for $m = 3$ and $m = 4$. We find that all $m \geqslant 3$ share the same dynamics of mode locking, with $m = 2$ being a special case due to the mathematical properties discussed in Sec. III B 1 (e.g., the independence of phase dynamics on amplitude).

The Arnold tongues for the critical Hopf regime have a noticeable difference between $m = 3$ and $m = 4$, with the tip of the tongue for the latter elevated above $F = 0$ (Fig. 10). This happens when y_2 function in Eq. (7) is of the same or higher order of X than the lowest-order term in y_1, which is the case when $m \geqslant 4$ for the critical Hopf regime ($\alpha = 0$,

$\beta_1 < 0$). The same rule applies to other regimes in the group represented by the critical Hopf regime (i.e., Group 1 in Table I). For the regimes for which the lowest-order term in y_1 is a constant term (i.e., $\alpha < 0$), the Arnold tongue is lifted off $F = 0$ when $m \geqslant 2$. When a quartic term is the lowest-order term in y_1 (i.e., $\alpha = \beta_1 = 0$, $\beta_2 < 0$), the Arnold tongue does not touch the F axis when $m \geqslant 6$.

IV. MODE LOCKING IN GRADIENT FREQUENCY NETWORKS

Now we study a GrFNN in which each oscillator receives the infinite-series input in Eq. (3) so that the network can mode lock to any input frequency (see Sec. II A). We first discuss frequency scaling for logarithmic frequency networks because logarithmic spacing is commonly used in the models of auditory neural processing and perception [22,31,32,41,42]. Then, we compare the widths of different mode-locking regions using approximations based on the analysis of individual modes. Finally, we compare the numerical simulations of a periodically forced GrFNN model with the analysis of individual modes.

A. Frequency scaling for logarithmic frequency networks

The analysis of individual modes showed above that canonical oscillators mode lock to external forcing when frequency difference Ω is small. Let Γ be the maximum $|\Omega|$ (or the upper bound) for which nonzero mode locking is possible for given parameter values. In other words, 2Γ is the width of the Arnold tongue for a given forcing amplitude. Since $\Omega = m\omega - k\omega_0$, the locking range $|\Omega| \leqslant \Gamma$ can be expressed as the range of natural frequency ω for given input frequency ω_0,

$$\frac{k\omega_0 - \Gamma}{m} \leqslant \omega \leqslant \frac{k\omega_0 + \Gamma}{m}, \qquad (12)$$

which is centered at $\frac{k}{m}\omega_0$ with the symmetrical half width of $\frac{\Gamma}{m}$. Note that the width of the natural frequency range does not vary with input frequency, that is, it is constant on a linear frequency scale.

As previously shown, scaling intrinsic and input parameters by natural frequency makes the locking range of a canonical oscillator increase width with natural frequency [28,29]. This property, called the "constant-Q" characteristic, is often desirable for oscillator networks and filter banks with logarithmically spaced frequencies because it makes each element in the system cover the same extent of logarithmic frequency space.

A frequency-scaled canonical oscillator with single-monomial input is given by

$$\tau\dot{z} = z\left(\alpha + 2\pi i + \beta_1|z|^2 + \frac{\epsilon\beta_2|z|^4}{1 - \epsilon|z|^2}\right) + \epsilon^{(k+m-2)/2}x^k\bar{z}^{m-1},$$

where $\tau = 1/f = 2\pi/\omega$ [28,29] [cf. Eq. (4)]. In polar coordinates,

$$\frac{1}{f}\dot{r} = \alpha r + \beta_1 r^3 + \frac{\epsilon\beta_2 r^5}{1 - \epsilon r^2} + \epsilon^{(k+m-2)/2}F^k r^{m-1}\cos\psi,$$

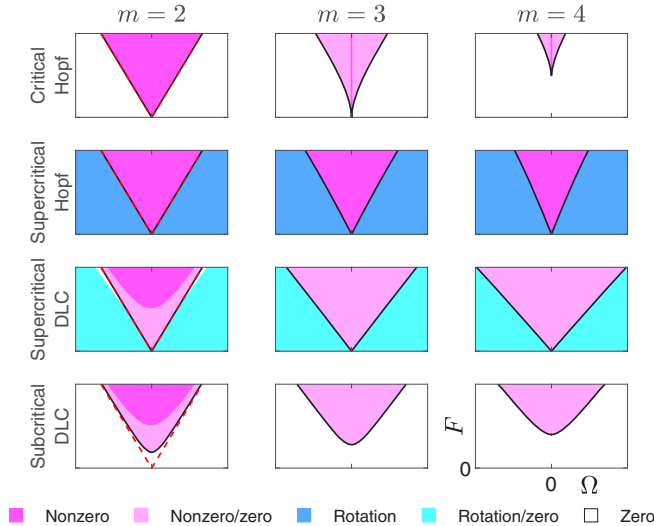$$\frac{1}{f}\dot{\psi} = \frac{\Omega}{f} - m\epsilon^{(k+m-2)/2}F^k r^{m-2}\sin\psi.$$

FIG. 10. Arnold tongues for $m = 2$, 3, and 4 for four representative regimes of intrinsic parameters. Black solid lines indicate the boundary of Arnold tongues obtained with Eq. (7), and red dashed lines show the locking regions for ψ given by Eq. (10) (for $m = 2$ only). Regions of the input parameter space (Ω, F) are colored by the set of attractors available at each point. For the grayscale version, see panel (a) of Figs. 2–9 for the letter labels for attractor sets.

Comparing with Eq. (5), we see that the steady-state equations $\dot{r} = 0$ and $\dot{\psi} = 0$ for a frequency-scaled oscillator are identical to the unscaled versions except that Ω is replaced with Ω/f. Hence, when $|\Omega| \leqslant \Gamma$ is the locking range for an unscaled oscillator, the locking range for the frequency-scaled version is $|\Omega/f| \leqslant \Gamma$ or $|\Omega| \leqslant f\Gamma$, which can be expressed as

$$\frac{k}{m + \frac{\Gamma}{2\pi}} \leqslant \frac{\omega}{\omega_0} \leqslant \frac{k}{m - \frac{\Gamma}{2\pi}} \quad (\text{if } \Gamma < 2\pi m),$$

$$\frac{\omega}{\omega_0} \geqslant \frac{k}{m + \frac{\Gamma}{2\pi}} \quad (\text{if } \Gamma \geqslant 2\pi m). \tag{13}$$

Since the ratio of natural frequency and input frequency has a fixed range, the width of locking range for a frequency-scaled oscillator is constant on a logarithmic frequency scale.

B. Comparison of mode-locking ranges

In general, low-order mode locking at a simple frequency ratio (i.e., with k and m being small integers) is stronger and more stable with a wider locking region than high-order mode locking at a more complex ratio (large k and m) [34]. This property of nonlinear resonance has been suggested to underlie the relative consonance and dissonance of musical intervals [21] and the tonal stability of pitches in musical keys [23,24]. In the latter studies, the coefficient to the input term in Eq. (4), $\epsilon^{(k+m-2)/2}$, was used as an estimate for the stability of mode locking in the $k : m$ ratio. Here we obtain an approximation of mode-locking ranges based on the analysis of individual modes presented above.

Equations (12) and (13) show the mode-locking ranges for unscaled and frequency-scaled canonical oscillators, respectively. However, it is not clear from these formulas how the width of locking region changes with k and m because Γ depends on k and m. To obtain a closed-form approximation of Γ, we assume that steady-state driven amplitude r^* is close to the spontaneous amplitude of the oscillator, which is a reasonable approximation for a supercritical Hopf oscillator driven by weak forcing. Then, from the steady-state equation $\dot{\psi} = 0$ for Eq. (5) we get

$$\Omega = m(\sqrt{\epsilon}F)^k (\sqrt{\epsilon}r_s)^{m-2} \sin \psi^*,$$

where r_s is the spontaneous amplitude of the oscillator. Since $|\sin \psi^*| \leqslant 1$, stable ψ^* exists when

$$|\Omega| \leqslant m(\sqrt{\epsilon}F)^k (\sqrt{\epsilon}r_s)^{m-2} \equiv \Gamma'. \tag{14}$$

Let us define

$$\gamma \equiv \frac{\Gamma'}{m} = (\sqrt{\epsilon}F)^k (\sqrt{\epsilon}r_s)^{m-2}.$$

Since $0 \leqslant \sqrt{\epsilon}F < 1$ and $0 \leqslant \sqrt{\epsilon}r_s < 1$ when the infinite-series RT is used (see Sec. II A), γ decreases as k and m increase, and $0 \leqslant \gamma < 1$ for $m \geqslant 2$. Using this approximation, the width of locking range for unscaled oscillators is

$$\frac{2\Gamma'}{m} = 2\gamma,$$

which is the difference of the upper and lower bounds in Eq. (12). The log-scale width of locking range for frequency-
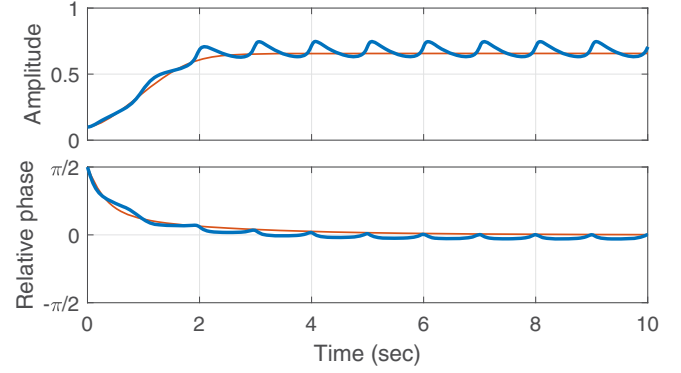

FIG. 11. Amplitude and relative phase of a canonical oscillator with the infinite-series input (thick blue lines) compared with a canonical oscillator with the 1:2 single-monomial input (thin red lines). The oscillators have identical intrinsic parameters (the natural frequency is 0.5 Hz), and they are driven by the same sinusoidal input of 1 Hz. The relative phase was computed for 1:2 locking, that is, $\psi = 2\phi - \theta$ where ϕ is oscillator phase and θ is input phase.

scaled oscillators is approximated to be

$$\log_b \frac{m + \frac{\Gamma'}{2\pi}}{m - \frac{\Gamma'}{2\pi}} = \log_b \frac{2\pi + \gamma}{2\pi - \gamma},$$

which is the difference of the logarithms of the upper and lower bounds in Eq. (13) for $m \geqslant 2$, where $b > 0$ is an arbitrary base. Thus, the approximated width of locking range decreases as k and m increase (because γ decreases) for both unscaled and frequency-scaled canonical oscillators, confirming the general property of nonlinear resonance that low-order mode locking is more stable than high-order mode locking.

C. Gradient frequency network with infinite series input

To study mode locking in the canonical model with infinite-series input, we numerically solved a frequency-scaled GrFNN model given by

$$\tau_i \dot{z}_i = z_i \left(\alpha + 2\pi i + \beta_1 |z_i|^2 + \frac{\epsilon \beta_2 |z_i|^4}{1 - \epsilon |z_i|^2} \right) + c \frac{x}{1 - \sqrt{\epsilon}x} \frac{1}{1 - \sqrt{\epsilon}\bar{z}_i}, \tag{15}$$

where $\tau_i = 2\pi/\omega_i$, ω_i is the natural frequency of the ith oscillator, c is additional coupling weight, and $x(t) = Fe^{i\omega_0 t}$ is sinusoidal forcing (see Sec. II B 4 for methods). As discussed above, the infinite series of input monomials allow a canonical oscillator to mode lock to an arbitrary input frequency.

Figure 11 compares an oscillator with the infinite-series input with an identical oscillator with a single resonant monomial. The natural frequency (0.5 Hz) and the input frequency (1 Hz) form a ratio of 1:2, thus the monomials with $k = n$ and $m = 2n$ in the series ($n \in \mathbb{N}$) become resonant and dominate the long-term dynamics of the oscillator. Unlike the oscillator with the single 1:2 resonant monomial (thin red lines), the amplitude and relative phase of the oscillator with infinite-series input (thick blue lines) do not converge to a fixed point due to the presence of nonresonant terms in the series. However, the relative phase is bounded and fluctuates
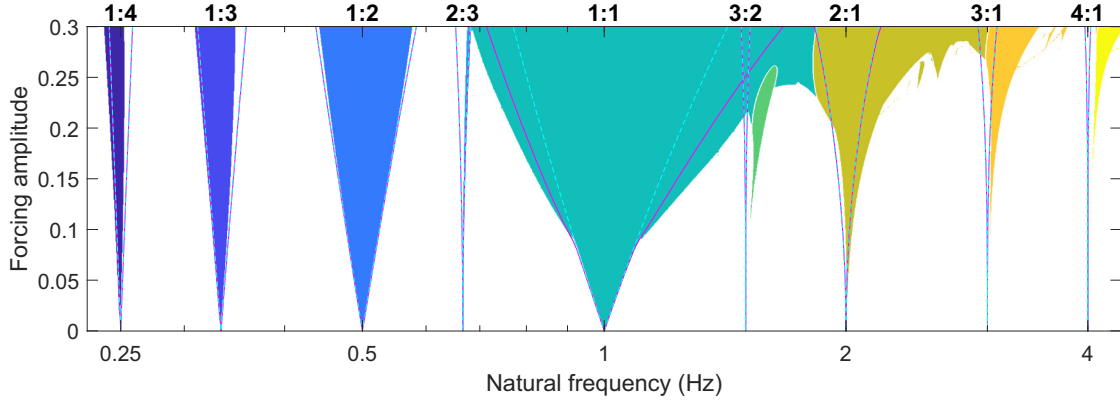
FIG. 12. Arnold tongues for a gradient frequency neural network driven by sinusoidal forcing in Eq. (15). Colored regions indicate frequency locking at different ratios. Solid magenta lines show the Arnold tongues from the analysis of individual modes calculated with Eq. (7), and dashed cyan lines show the closed-form approximation of locking ranges in Eq. (14). The input frequency is 1 Hz, and the oscillators are in the supercritical Hopf regime ($\alpha = 0.9$, $\beta_1 = -3$, $\beta_2 = -3$, $\epsilon = 1$, $c = 3$). The Arnold tongues were obtained by running 2001 oscillators, with natural frequencies equally spaced on a log scale from 0.23 to 4.4 Hz, 1001 times for different forcing amplitudes ranging from 0 to 0.3 (see Sec. II B 4 for methods).

around the fixed point for the single-monomial oscillator [i.e., the trajectory forms a libration in (r, ψ), not a rotation (see [29,35])]. Hence, when averaged over a long enough time scale, the infinite-series oscillator has the same instantaneous frequency as the single-monomial oscillator. This type of synchronization may be called "frequency locking" instead of mode locking [34].

Figure 12 shows the Arnold tongues for the GrFNN model with infinite-series input in Eq. (15), identified by the time-averaged instantaneous frequencies of the oscillators (see Sec. II B 4 for methods). Only the tongues for low-order resonances with $k + m \leqslant 5$ are displayed as colored regions. Consistent with the analysis of individual modes, the GrFNN model with infinite-series input has wider Arnold tongues for low-order resonances (with small k and m) than for higher-order resonances (larger k and m). At low forcing amplitudes, the tongues for canonical oscillators with single-monomial input (solid magenta lines; from Sec. III) match the tongues for infinite-series input (colored regions). For stronger forcing, the tongues for infinite-series input are tilted and deviate from the tongues for single-monomial input, indicating that long-term oscillator dynamics are influenced by multiple resonant monomials for distinct mode-locking ratios. A detailed analysis of the canonical model with infinite-series RT is beyond the scope of this paper, which we leave for future work.

Note that for $k \geqslant 1$ and $m = 1$, the tongues for infinite-series input (colored regions in Fig. 12) are significantly wider than the tongues for single-monomial input (magenta solid lines) at high forcing amplitudes. This is expected given that the oscillators are in the supercritical Hopf regime, for which a region of frequency locking (i.e., libration) exists just outside the mode-locking range for strong forcing [29]. As discussed in Sec. IV B, the tongues for individual modes (magenta solid lines) and their approximations in Eq. (14) (cyan dashed lines) match well at low forcing amplitudes because driven amplitudes are close to the spontaneous amplitude. They deviate at higher forcing amplitudes for which the driven amplitudes at locking boundaries are significantly different from the spontaneous amplitude.

V. CONCLUSION

We examined mode locking in periodically forced gradient frequency neural networks by analyzing a canonical model. As in our previous analysis of 1:1 phase locking [29], we found that the canonical model has different sets of attractors in four representative parameter regimes. We studied individual modes of locking separately by analyzing the canonical model with single-monomial input. We found that harmonic locking ($k \geqslant 2$, $m = 1$) has qualitatively identical dynamics to 1:1 phase locking. Among subharmonic ratios, $m = 2$ has distinct properties from $m \geqslant 3$ due to the independence of phase dynamics on amplitude. Using a closed-form approximation, we showed that the width of Arnold tongue (i.e., locking region) for $k : m$ mode locking decreases as k and m increase, indicating low-order nonlinear resonances are generally more stable than higher-order ones. Finally, we examined the Arnold tongues for the canonical model with infinite-series input which is capable of mode locking to an arbitrary input frequency. For weak forcing, the Arnold tongues for infinite-series input match the tongues for single-monomial input, but they deviate as forcing amplitude increases because multiple input monomials affect oscillator dynamics at high forcing amplitudes.

The analysis presented in this paper has broad implications for neural processing and nonlinear dynamics. The canonical model analyzed here is a generic mathematical model of tonotopically organized neural networks, which are commonly found in the auditory system. Thus, the properties of mode locking found in the canonical model are relevant to auditory neural processing and perception in general. Our previous modeling studies showed that mode-locked resonances in neural oscillators can explain nonlinear components in human auditory brainstem responses to musical intervals [31], and the perception of harmony [22], tonality [24], and rhythm and meter in music [27]. The present analysis provides mathematical foundations to these studies. Also, by presenting the complete set of driven behaviors available to the canonical model, this study informs modeling efforts featuring the GrFNN

model [38] as to choosing appropriate parameter regimes and values to achieve target behaviors.

Compared to biological neuron models such as the Hodgkin-Huxley model, the canonical model is mathematically simpler and more tractable, and hence we were able to analyze and compare different modes of synchronization for all parameter regimes available in the model. The thorough analysis given in this paper can serve as a canonical reference for diverse mode-locking behaviors observed in neurons and neuron models which are often difficult to control and analyze (e.g., [4–7,9–12]). Lastly, since the canonical model is a generic model of nonlinear oscillatory networks, the present analysis is not limited to neural networks but applies generally to multifrequency nonlinear systems consisting of oscillatory elements poised near a Hopf bifurcation or a Bautin bifurcation. In this light, the present study reveals the signal processing capabilities of multifrequency nonlinear systems by showing how they transform external signals into spatiotemporal patterns of synchronized activities.

[1] M. H. Jensen, P. Bak, and T. Bohr, Phys. Rev. A **30**, 1960 (1984).

[2] J. E. Flaherty and F. C. Hoppensteadt, Stud. Appl. Math. **58**, 5 (1978).

[3] N. H. Fletcher, J. Acoust. Soc. Am. **64**, 1566 (1978).

[4] K. Aihara, T. Numajiri, G. Matsumoto, and M. Kotani, Phys. Lett. A **116**, 313 (1986).

[5] N. Takahashi, Y. Hanyu, T. Musha, R. Kubo, and G. Matsumoto, Physica D (Amsterdam, Neth.) **43**, 318 (1990).

[6] M. R. Guevara, L. Glass, and A. Shrier, Science **214**, 1350 (1981).

[7] M. R. Guevara, A. Shrier, and L. Glass, Am. J. Physiol.-Heart Circ. Physiol. **254**, H1 (1988).

[8] A. Szűcs, R. C. Elson, M. I. Rabinovich, H. D. I. Abarbanel, and A. I. Selverston, J. Neurophysiol. **85**, 1623 (2001).

[9] S.-G. Lee and S. Kim, Phys. Rev. E **60**, 826 (1999).

[10] S.-G. Lee and S. Kim, Phys. Rev. E **73**, 041924 (2006).

[11] K. Yoshino, T. Nomura, K. Pakdaman, and S. Sato, Phys. Rev. E **59**, 956 (1999).

[12] G. Baier, T. Hermann, and M. Muller, in *Ninth International Conference on Information Visualisation (IV '05)* (IEEE, London, England, 2005), pp. 5–10.

[13] A. A. Farokhniaee and E. W. Large, Phys. Rev. E **95**, 062414 (2017).

[14] J. P. Keener, F. C. Hoppensteadt, and J. Rinzel, SIAM J. Appl. Math. **41**, 503 (1981).

[15] S. Coombes and P. C. Bressloff, Phys. Rev. E **60**, 2086 (1999).

[16] Tonotopic organization refers to the spatial arrangement of processing units by characteristic frequency. It is found in all levels of auditory processing, from the cochlea to the auditory cortex.

[17] E. W. Large, J. R. Kozloski, and J. D. Crawford, in *Association for Research in Otolaryngology Abstracts* (1998), Vol. 21, p. 717.

[18] J. Laudanski, S. Coombes, A. R. Palmer, and C. J. Sumner, J. Neurophysiol. **103**, 1226 (2010).

[19] K. M. Lee, E. Skoe, N. Kraus, and R. Ashley, J. Neurosci. **29**, 5832 (2009).

[20] J. H. E. Cartwright, D. L. González, and O. Piro, Proc. Natl. Acad. Sci. U.S.A. **98**, 4855 (2001).

[21] I. Shapira Lots and L. Stone, J. R. Soc. Interface **5**, 1429 (2008).

[22] J. C. Kim, Frontiers Psychol. **8**, 666 (2017).

[23] E. W. Large, in *Nonlinear Dynamics in Human Behavior*, edited by R. Huys and V. K. Jirsa (Springer, Berlin, Heidelberg, 2010), pp. 193–211.

[24] E. W. Large, J. C. Kim, N. K. Flaig, J. J. Bharucha, and C. L. Krumhansl, Music Percept. **33**, 319 (2016).

[25] E. W. Large and J. F. Kolen, Connect. Sci. **6**, 177 (1994).

[26] E. W. Large, in *Psychology of Time*, edited by S. Grondin (Emerald, Bingley, UK, 2008), pp. 189–232.

[27] E. W. Large, J. A. Herrera, and M. J. Velasco, Front. Syst. Neurosci. **9**, 159 (2015).

[28] E. W. Large, F. V. Almonte, and M. J. Velasco, Physica D (Amsterdam, Neth.) **239**, 905 (2010).

[29] J. C. Kim and E. W. Large, Front. Comput. Neurosci. **9**, 152 (2015).

[30] F. C. Hoppensteadt and E. M. Izhikevich, in *The Handbook of Brain Theory and Neural Networks*, 2nd ed., edited by M. A. Arbib (MIT Press, Cambridge, MA, 2001), pp. 181–186.

[31] K. D. Lerud, F. V. Almonte, J. C. Kim, and E. W. Large, Hear. Res. **308**, 41 (2014).

[32] K. D. Lerud, J. C. Kim, F. V. Almonte, L. H. Carney, and E. W. Large, in *Association for Research in Otolaryngology Absracts*, (2015), Vol. 38, pp. 211–212.

[33] Dynamical systems analyses of other components in the canonical model, including mutually coupled oscillators and plastic connections, will be given in separate papers.

[34] F. C. Hoppensteadt and E. M. Izhikevich, *Weakly Connected Neural Networks*, Applied Mathematical Sciences No. 126 (Springer-Verlag, New York, 1997).

[35] S. H. Strogatz, *Nonlinear Dynamics and Chaos: With Applications to Physics, Biology, Chemistry, and Engineering* (Perseus Books, Cambridge, MA, 1994).

[36] P. L. Boyland, Commun. Math. Phys. **106**, 353 (1986).

[37] A. Pikovsky, M. Rosenblum, and J. Kurths, *Synchronization: A Universal Concept in Nonlinear Sciences* (Cambridge University Press, Cambridge, 2001).

[38] E. W. Large, J. C. Kim, K. D. Lerud, and D. Harrell, GrFNN Toolbox: MATLAB tools for simulating signal processing, plasticity and pattern formation in gradient frequency neural networks, https://github.com/MusicDynamicsLab/GrFNNToolbox, 2014.

[39] R. Adler, Proc. IRE **34**, 351 (1946).

[40] Detailed steps for solving the equation are given in Sect. 4.3 of [35].

[41] R. Meddis and L. O'Mard, J. Acoust. Soc. Am. **102**, 1811 (1997).

[42] S. A. Shamma and D. Klein, J. Acoust. Soc. Am. **107**, 2631 (2000).